MODELLING OF FLOW OVER THE ALPS

by Terry L. Clark

National Center for Atmospheric Research [1]
Boulder, Colorado 80307

1. INTRODUCTION

Mountains can exert a frictional force on the atmosphere which is usually treated using a drag law formulation at the earths physical surface. This type of force is similar to that experienced over flat terrain in that it acts locally. There are also the forces due to stable air flowing over and diverted around the mountains. The pressure drag and remote gravity wave drag (GWD) have become recognized as important to the general circulation problem by Bretherton (1969) and Lilly (1972) among others. In recent years, marked improvements to both forecast quality and model 'climates' have resulted from using enhanced orographies such as 'envelope' or 'silhouette' ones, and most recently by parameterizing the dynamics of subgridscale gravity waves excited by flow over irregular terrain (Palmer et al., 1986; Boer et al., 1984)

Generally modellers have used linear wave theory and idealized two–dimensional flow solutions to guide the design of their GWD parameterization. Parameterization schemes must formulate an effective surface stress due to the presence of gravity waves and define a three–dimensional spatial distribution of this stress. There is also a considerable heuristic element in the formulation of the gridpoint orography.

It has become possible to perform fully three–dimensional non–hydrostatic flows over realistic orography due to increased computer power and interactive gridnesting software which allows very high resolution within the area of interest. The gridnesting model of Clark and Farley (1984) which was developed from the model of Clark (1977) has been applied to flow over the Alps for the 8 Nov 1982 foehn event. The simulations of the flow over the front range of the Colorado Rockies for the windstorm event of 9 Jan 1989 will also be discussed.

[1] The National Center for Atmospheric Research is sponsored by the National Science Foundation

boundary conditions have been important components affecting our thinking about this subject. Briefly, the linear boundary condition is

$$w\Big|_{z=0} = U\Big|_{z=0}\frac{\partial h}{\partial x} + V\Big|_{z=0}\frac{\partial h}{\partial y} \tag{1}$$

whereas the so–called 'non–linear' boundary condition (Vergeiner, 1971) is

$$w\Big|_{z=h} = U\Big|_{z=h}\frac{\partial h}{\partial x} + V\Big|_{z=h}\frac{\partial h}{\partial y} \tag{2}$$

where in both (1) and (2) $U = U(z)$ and $V = V(z)$. Clearly, both (1) and (2) are linear equations and it is unfortunate that such misleading jargon as 'non–linear' boundary condition for (2) has come into common use. In terms of horizontal Fourier representation (1) is separable whereas (2) is non–separable. (2) considers effects of finite amplitude. There are some well known amplification effects of finite amplitude mountains. These have been discussed by Miles and Huppert (1969), Smith (1976), Lilly and Klemp (1979), Peltier and Clark (1979), among others. An example of such a finite amplitude effect is the pressure drag associated with hydrostatic flow over the bell–shaped mountain $h(x) = h_0/(1+(x/a)^2)$ which for hydrostatic theory is given by Miles and Huppert (1969) as

$$D_0 = \frac{\pi N h^2 U}{4}[1 + \frac{7}{16}(Nh/U)^2 + ...] \tag{3}$$

where the term inside the [ ] brackets represents the difference between the linear solutions satisfying (1) and those satisfying (2). Effects of mountain shape on the pressure drag have also been discussed. The finite amplitude aspect of linear theory which I want to address here is the issue of *effective orography* as it relates to possible non–hydrostatic forcing.

Effective orography, h_{eff}, is defined as that orography which satisfies the linearly separable boundary condition (1) and at the same time satisfies the non–separable boundary condition (2) for the actual orography, h. h_{eff} is a function of (h, U, V, N, ρ, x, y). It is of interest in that it describes the orography for the linearly separable problem. It is the linear separable problem which is by far the most easily understood and in fact usually referred to as simply the linear problem. If, for example, there are scales of forcing in h_{eff} which are appropriate for lee wave formation then

2. OBSERVATION AND MODEL COMPARISONS OF PRESSURE AND GRAVITY WAVE DRAG

Hoinka and Clark (1991) compared model simulations of the airflow over the Alpine complex for the 8 Nov 1982 foehn event with observations. The total pressure drag from the model was -4.7 and 1.7 $\times$ 10^{11} N for the meridional and zonal values. These values compare reasonably well with the values of -4.3 and 1.8 $\times$ 10^{11} N which were observed during ALPEX for four foehn events. There were no measurements of pressure drag for the entire Alps on 8 Nov 1982 as the ALPEX experiment had ended.

There were observations of both pressure drag and momentum flux on 8 Nov 1982 between Vicenza and Munich. The observed pressure drag was -.67 $\times$ 10^6 N m^{-1} and the model simulated value was -.62 $\times$ 10^6 N m^{-1} using 5 km horizontal resolution. This comparison is quite good particularly considering that the simulation employed horizontally uniform upstream mean wind and stability profile initial conditions which was an approximation of the observed jet structure. The comparisons between the observed and simulated momentum fluxes was not at all close. The observations showed an average flux of -.75 $\times$ 10^5 N m^{-1} between 5 and 10 km above msl whereas the model produced -.50 $\times$ 10^6 N m^{-1} which is almost 7 times larger than the observed value.

A number of possible reasons for the poor comparison between the simulated and observed momentum fluxes were discussed. These included; 1) idealized upstream conditions; 2) lack of surface friction in the simulations; 3) strong horizontal variability of Reynolds stress resulting in questionable representativeness of a single cross–section; 4) difficulties in measuring momentum fluxes; 5)non–hydrostatic effect; or a combination of the above. As will be discussed in this paper, surface friction might be able to account for as much as half of the difference. Nevertheless, the comparisons described in Hoinka and Clark (1991) indicate that there is a need to significantly improve the observation/simulation comparison studies.

3. EFFECTIVE OROGRAPHY: A FINITE AMPLITUDE EFFECT IN LINEAR THEORY

Linear theory has long proven useful for analysing various aspects of stable air flow over two- and three–dimensional orography. The linear and so–called 'non–linear'

we should expect to see lee waves in the solutions of flow over the mountain shape h. On the other hand, if we were to ignore finite amplitude effects then h could be heavily enough filtered to suggest that lee wave activity should be insignificant.

Effective orography can be calculated using matrix techniques similar to those employed by Chen and Trenberth (1988). Consider the simple steady state gravity wave problem described by the hydrostatic wave equation

$$\frac{\partial \hat{w}_{k,\ell}}{\partial z^2} + c^2 \hat{w}_{k,\ell} = 0 \tag{4}$$

where $\hat{w}_{k,\ell}$ represents the Fourier transform of w such that $w(x,y,z) = \sum_{k,\ell} \hat{w}_{k,\ell}(z) e^{i(kx+\ell y)}$. The vertical structure for each Fourier component can be solved and represented in terms of the $z = 0$ value of the coefficient and w represented as $w(x,y,z) = \sum_{k,\ell} \hat{w}_{k,\ell}(z=0)\tilde{w}_{k,\ell}(z) e^{i(kx+\ell y)}$ where we have reduced the unknown in w to the surface value of $\hat{w}$ or $\hat{w}_{k,\ell}(z=0)$. Similar representations are easily found for the other perturbation components u and v. A matrix equation can be found for the free–slip linear model from the equation

$$w\Big|_{z=h} = (U+u)\Big|_{z=h} \frac{\partial h}{\partial x} + (V+v)\Big|_{z=h} \frac{\partial h}{\partial y} \tag{5}$$

which simply states that no air is allowed to flow through the physical mountain. Substituting the relations

$$\hat{w}_{k,\ell}(z) = \hat{w}_{k,\ell}(0)\tilde{w}_{k,\ell}(z)$$

$$\hat{u}_{k,\ell}(z) = \hat{w}_{k,\ell}(0)\tilde{u}_{k,\ell}(z)$$

$$\hat{v}_{k,\ell}(z) = \hat{w}_{k,\ell}(0)\tilde{v}_{k,\ell}(z)$$

into (5) results in a fully packed matrix of order equal to the total number of wavenumber components. The unknowns in the matrix equation are the values of $\hat{w}_{k,\ell}(z=0)$. Once the matrix is solved the solution satisfying (2) is known. The effective orography is found by substituting the solution to (2) into (1) and solving for h which will in this case be h_{eff}.

An extreme example of h_{eff} is the flow over the island of Hawaii. The hydrostatic linear equations were solved for the case of a 500 m deep neutral boundary

layer with $N = .01$ aloft. The airflow is assumed to be from the east at 10 m s^{-1} at all heights. The air density was given a scale height of 10 km. Figure 1 shows east–west cross sections of u, v, w and θ at a near center position of the island. We can see that the flow reversal is extreme and we have far exceeded the conditions under which we might expect linear theory to apply. Fig. 2 shows plots of w and θ on the surface, $z = h$, for the entire domain. One sees the typical drag character of w expected from linear theory, i.e. mild updrafts on the upstream side of the mountain with stronger lee side downdrafts. θ is not uniform on the surface for this solution as this has not been enforced as a constraint. A constant surface θ field should result if an upstream absorber where used to mimic infinite domain effects similar to the procedure used by Laprise and Peltier (1989). Fig. 2 shows the actual orography used to form the matrix equation where 10 km horizontal resolution was used in this case (matrix order was 1600). Fig. 3 shows a plot of the effective orography for this case where the variation is $\approx \pm 8$ km. Visual inspection of h_{eff} in Fig. 3 indicates a very different spectral distribution of h_{eff} than that in h. There is a rather noticeable proboscisity to the solution of the linear flow equations over Hawaii. In Fig. 3 the horizontal wind vectors are also plotted but for the level $z = 750$ m which is just above the top of the boundary layer. Notice how the proboscisity of the flow has resulted in a downstream convergence zone in the lee of the island. This convergence zone is a direct result of linear hydrostatic gravity wave forcing as the plots did not change significantly for the case of zero Coriolis force.

The previous example was presented as an extreme example to emphasize the finite amplitude effect of orography on the effective shape of the orography. (It also gave me the opportunity to use the term *proboscisity* which I have never used in a paper before.) The same concept can be applied to the Alps complex to better understand their effective shape for some particular flow regime. Some preliminary linear calculations were performed on the Alps complex. The horizontal resolution was set to 40 by 40 km with 50 by 50 grid points in the x- and y–directions. The shape of the Alps was modified near their periphery to allow for cyclic representation. The order of the matrix equation representing the non–separable boundary condition was 2500. The same wind and stability profiles as in Hoinka and Clark (1991) and Clark and Miller (1991) was used. The linear code is still a bit flaky and results will be

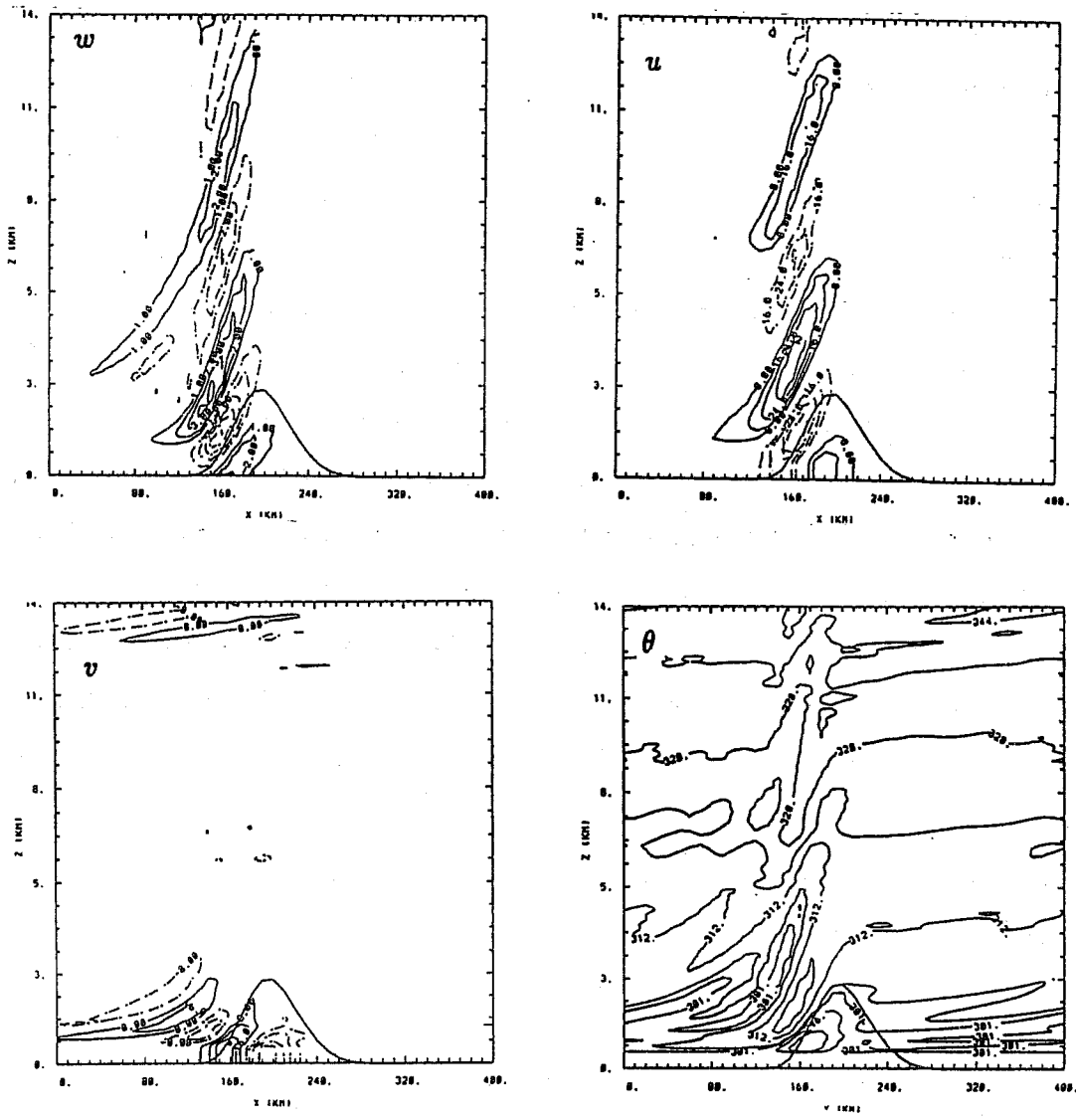

Fig. 1 East–west cross–sections of w, u, v, and θ for the steady–state linear solutions of flow over Hawaii.

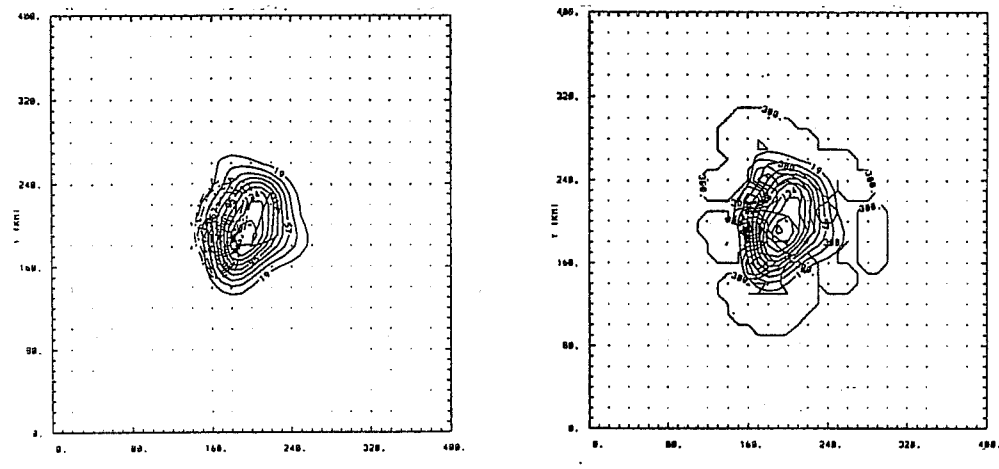

Fig. 2 Surface plots of a) w and b) θ from the case shown in Fig. 1. Horizontal winds are shown for z =0.

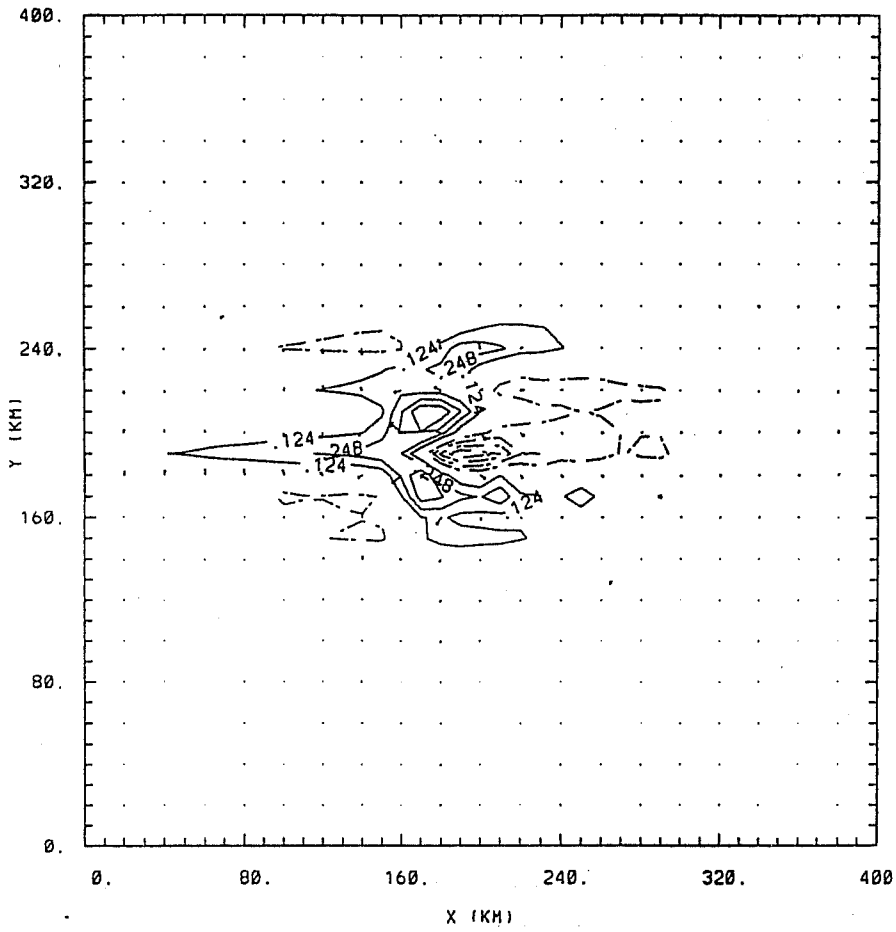

Fig. 3 Plot of effective orography for case shown in Fig. 1. Horizontal winds are shown for z= 750 m.

shown only if some remaining problems are overcome.

4. EFFECT OF SURFACE FRICTION: SOME PRELIMINARY RESULTS.

Clark and Miller (1991) as an extension of the work of Hoinka and Clark (1991) performed a series of simulations of airflow over the Alps complex for the 8 Nov 1982 foehn case. All except one of their experiments used free slip lower boundary conditions. One of the free slip experiments was rerun using a surface drag formulation with $C_D = .001$ where the surface stress, $\vec{\tau}_{sfc}$, was represented as

$$\vec{\tau}_{sfc} = C_D|\vec{V}|\vec{v}. \tag{6}$$

The resolution was 10 km in the horizontal and 500 m in the vertical for the inner domain. The pressure drag and Reynolds stress are shown in Figs. 4 and 5 for both the case with C_D =0 and C_D =.001. Fig. 4 displays the pressure drag versus time and shows that the pressure drag is reduced by about 8% due to the effect of including surface drag. This result is in agreement with the results of Richard et al. (1989). However, Fig. 5 indicates a rather interesting result for the partitioning of the pressure drag. The heavy dots at the bottom of Fig. 5(a) represent the pressure drag values for each of the experiments. They are placed at z=0 simply for convenience and the dotted lines joining up the pressure drag with the Reynolds stress aloft are only there to indicate which drags go with which stresses. The pressure drag difference is the 8% referred to in Fig. 4. The difference in Reynolds stress is 24% which is a factor of 3 larger than for the surface pressure drag effect.

The significant decrease in wave drag due to such a small value of C_D is probably due to the surface friction diverting a deeper layer of fluid around the Alps in the case of C_D= .001. As discussed by Bretherton (1969), among others, it is

$$< \rho u'w' - \rho f v'\zeta >$$

and

$$< \rho v'w' + \rho f u'\zeta >$$

which are conserved where ζ is the free stream deflection height. The $<\ >$ operator indicates a horizontal average. Another possibility is that the effect of surface friction

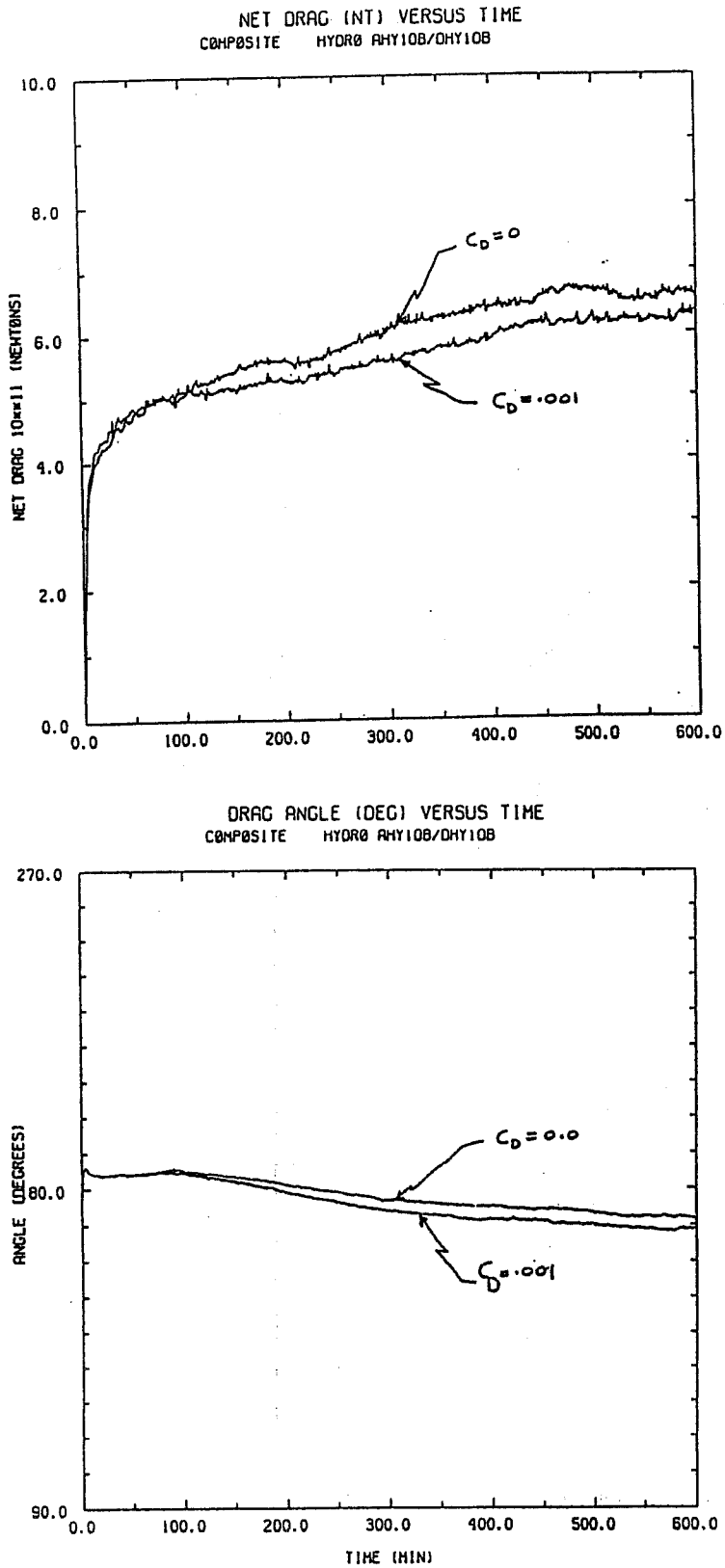

Fig. 4 Pressure drag versus time for 8 Nov 1982 Alps foehn event. Results for surface drag coefficient, $C_D = 0$ and .001 are shown. Both experiments used $\Delta x = \Delta y =$ 10 km.

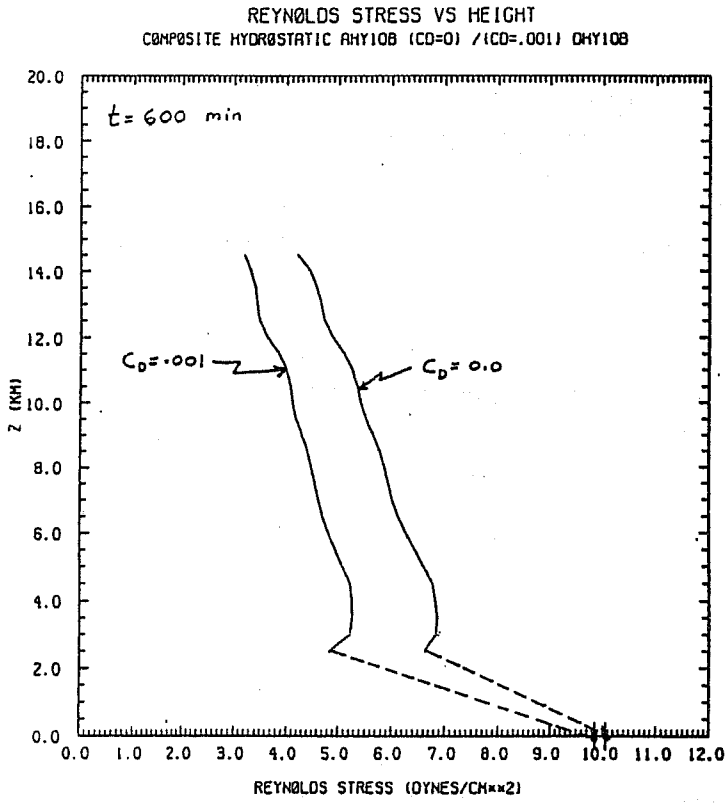

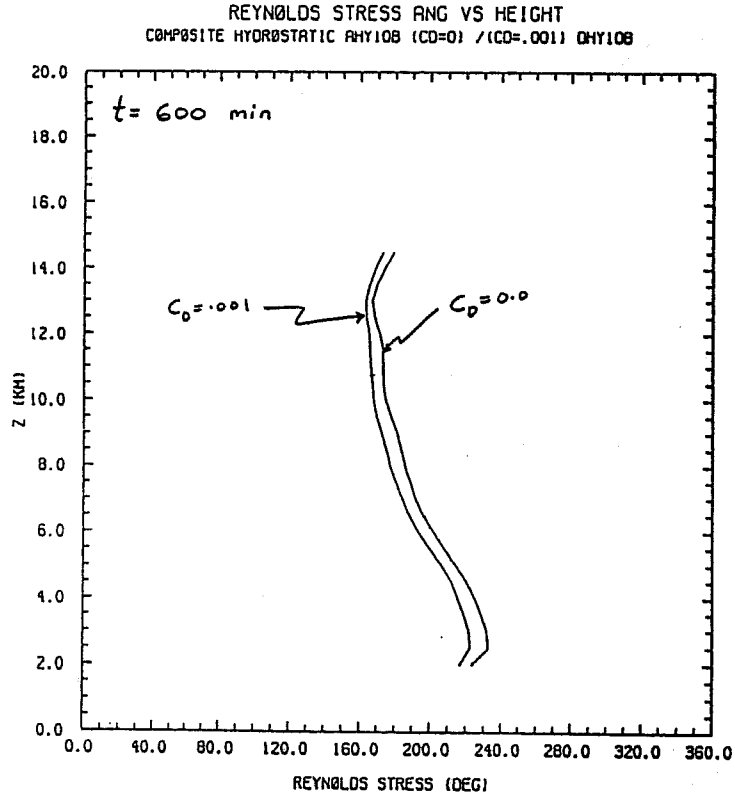

Fig. 5 Profiles of Reynolds stress versus height at t= 600 min for the two cases shown in Fig. 4. Heavy dots at z =0 denote surface pressure drag values. Dashed lines are drawn only to denote which drag goes with which stress.

is to produce a viscous component of the pressure drag which tends to increase it while at the same time the friction decreases the gravity wave component. The net effect is then, perhaps, a minor decrease in the pressure drag due to surface friction. One way to assess this possible effect is to run a case in an $N = 0$ atmosphere with $C_d \neq 0$ to estimate the frictional component of the drag.

One of the purposes for developing the linear model was for purposes of analyzing the partitioning of the pressure drag for the flow around the Alps. A better understanding of this partitioning seems important to the gravity wave drag parameterization problem. Recent developments in the Clark model are also directed at better explicit treatments of surface friction effects. The vertical stretching will be used to attempt to assess differences between free slip and no slip treatments of airflow over mountain complexes.

5. EFFECT OF HORIZONTAL RESOLUTION AND HYDROSTATIC ASSUMPTION ON PRESSURE AND WAVE DRAG

The previous analysis suggests that the finite amplitude effect of the orography should result in significant gravity wave excitation at all horizontal scales resolved by the finite difference nonlinear model. The potential exits, then, for such phenomena as trapped lee waves to occur in the non-hydrostatic model which could affect the pressure and wave drags as compared with the hydrostatic model estimates. As will be discussed, these type of effects did not appear to be significant even at the 5 km horizontal grid sizes. One reason why such effects did not appear significant in either the Hoinka and Clark (1991) or Clark and Miller (1991) simulations is that the effects of the ∇^6 horizontal filter were perhaps sufficient to suppress any such resonant modes for the marginal horizontal resolution.

The two-dimensional analysis of Keller et al. (1991) shows a significant difference between the horizontal structures of the hydrostatic and nonhydrostatic Reynolds stresses. They analyzed the stresses in terms of horizontal running averages in order to isolate downstream effects due to the existence of lee waves in the nonhydrostatic system. Figure 6 shows plots of the running average momentum fluxes. The average fluxes converge to similar values far downstream but this distance can be

a number of large scale model grid points ($\approx$ 200 km). The differences in the flux results seen in Fig. 6 are due to the existence of leaky resonant modes or lee waves in the nonhydrostatic case. An example of their wave solutions is shown in Fig. 7.

Clark and Miller (1991) performed a series of experiments of airflow over the Alps with horizontal resolutions of 80, 40, 20, 10 and 5 km. These experiments were also performed in both non–hydrostatic and hydrostatic framework. Figure 8 shows a plot of pressure drag versus time over a domain of 800 by 640 km in the x- and y–directions, respectively. This figure shows the near steady–state result from both the non–hydrostatic and hydrostatic calculations. At these resolutions we see very minor but systematic differences due to the hydrostatic assumption. The hydrostatic system under estimates the pressure drag by a few percent as compared with the non–hydrostatic model. The most significant information in this figure is the resolution dependence of the pressure drag on horizontal resolution. The drag has reached a (perhaps local) asymptote at about 20 km horizontal resolution. The 80 km result is a little less than a factor of two smaller than the asymptotic value. Figure 9 shows both the pressure drag values corresponding to Fig. 8 and the Reynolds stress profiles for the same cases. It is interesting to note that the Reynolds stress profiles show an even larger variation due to horizontal resolution than does the pressure drag.

6. EFFECT OF ENVELOPE OROGRAPHY

Also plotted on Fig. 9 is the envelope calculations for the 80 and 40 km horizontal resolution cases. The envelope was calculated using a mean 5 km resolution data set for the entire outer domain of the Alpine complex. A one standard deviation from the 5 km data set was added to the lower resolution mean orography to produce the respective envelope orography. This is similar to the procedure followed by Mesinger and Strickler (1982) and Wallace et al. (1983). A gravity wave drag parameterization had not been considered in these calculations. As a result of the inclusion of the simple envelope orography the pressure drag magnitude was considerably improved. The 80E case almost attained the 40 km value and the 40E case similarly almost attained the 20 km value. The Reynolds stress profiles were improved due to the inclusion of the envelope but showed significantly less improvement than

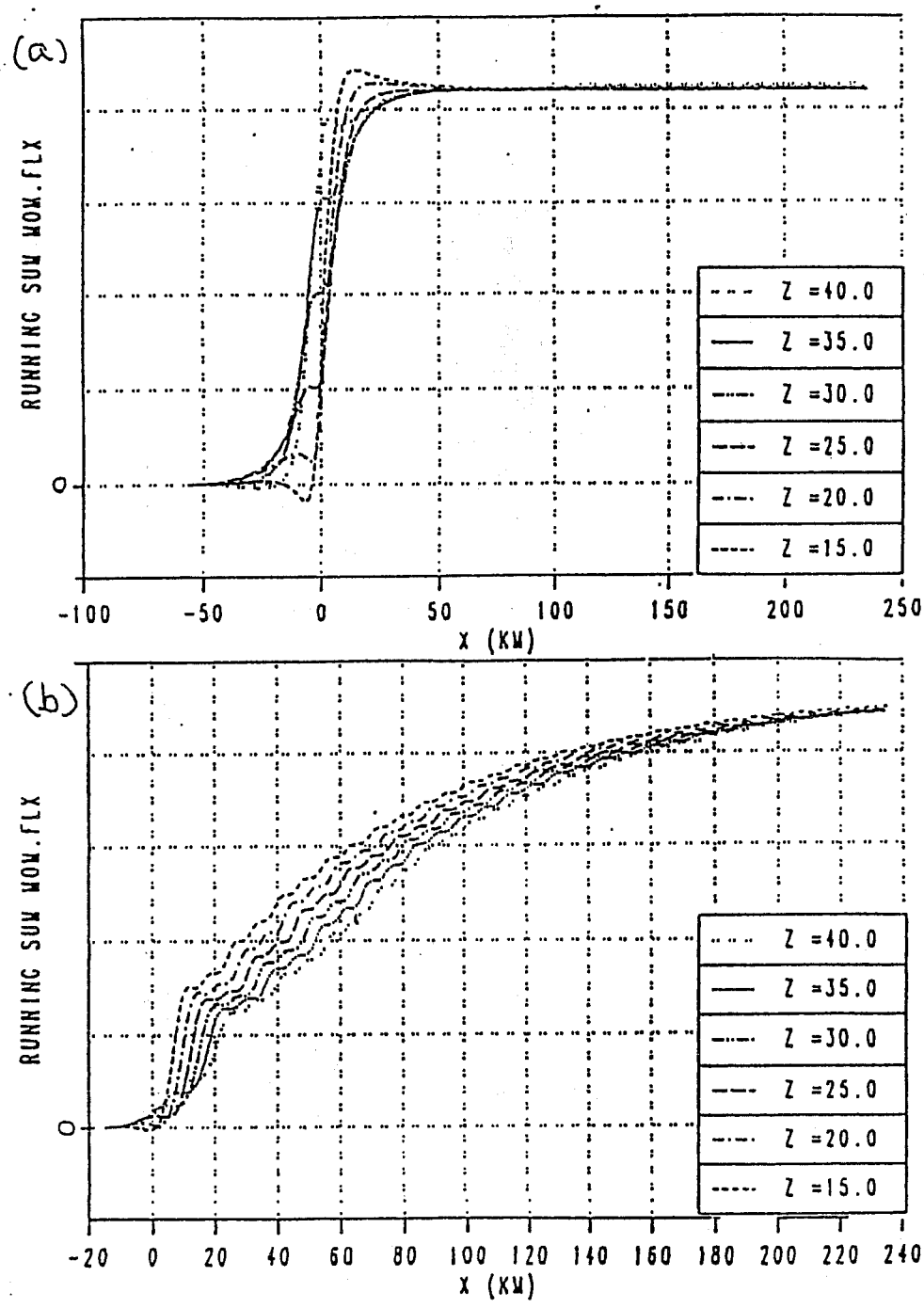

Fig. 6 Running sum of momentum flux, $u'w'$ for 6 different heights for (a) hydrostatic and (b) nonhydrostatic waves. (From Keller et al. 1991)

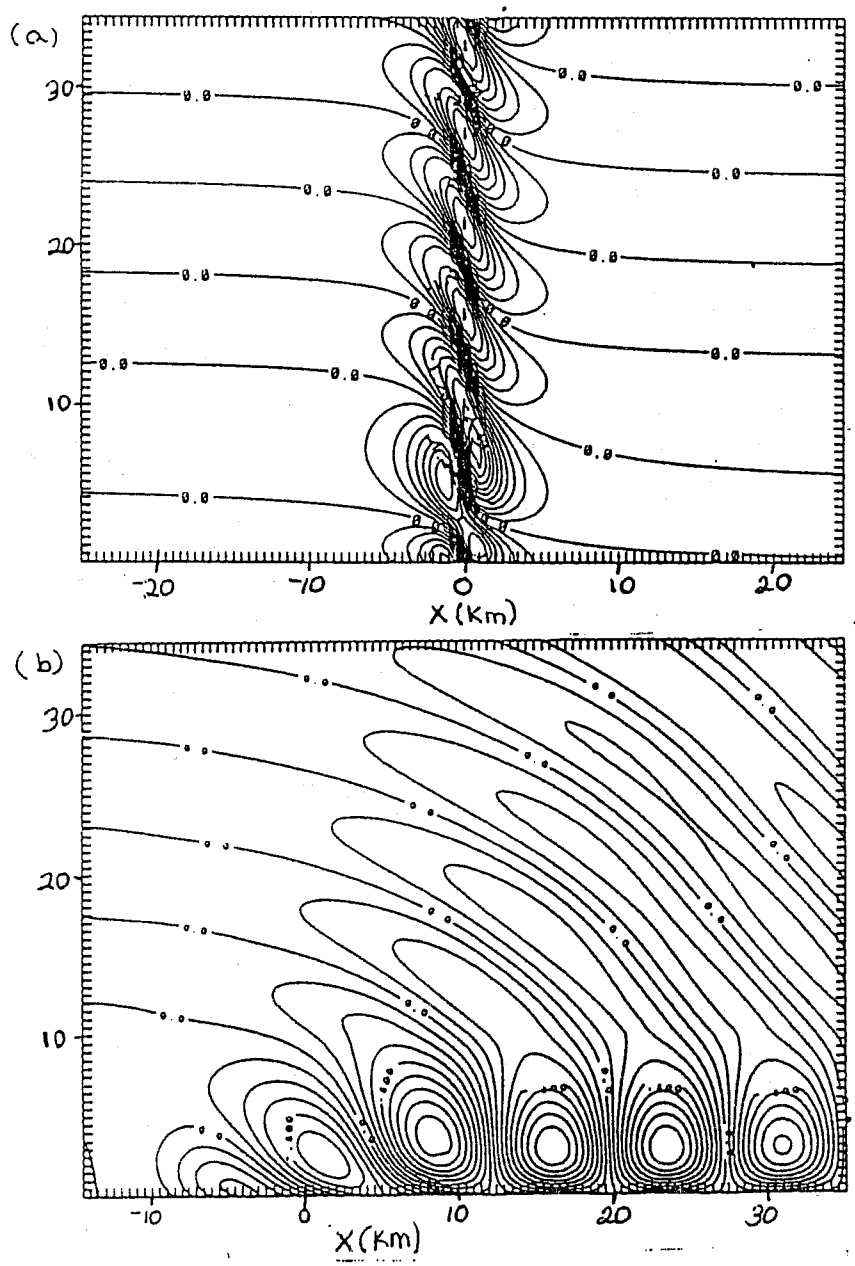

Fig. 7. Contours of vertical velocity for air flow over a 2 km half–width mountain; (a) hydrostatic solution, (b) nonhydrostatic solution. (From Keller et al. 1991)

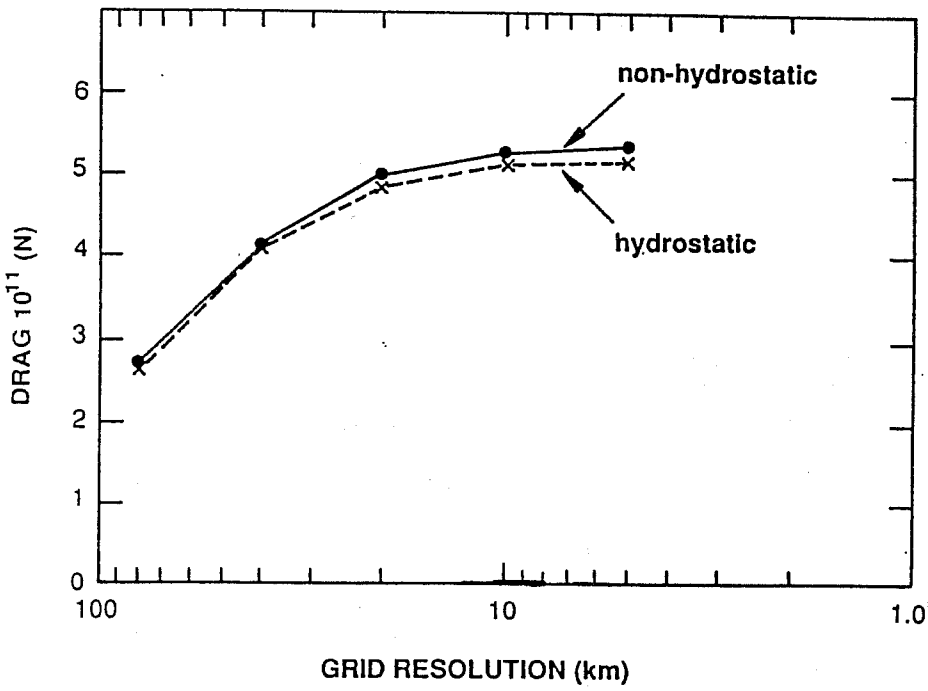

Fig. 8 Steady–state pressure drag versus horizontal resolution for flow over the Alps. Results derived from solutions over an 800 × 640 km domain. Both hydrostatic and non-hydrostatic results are shown.

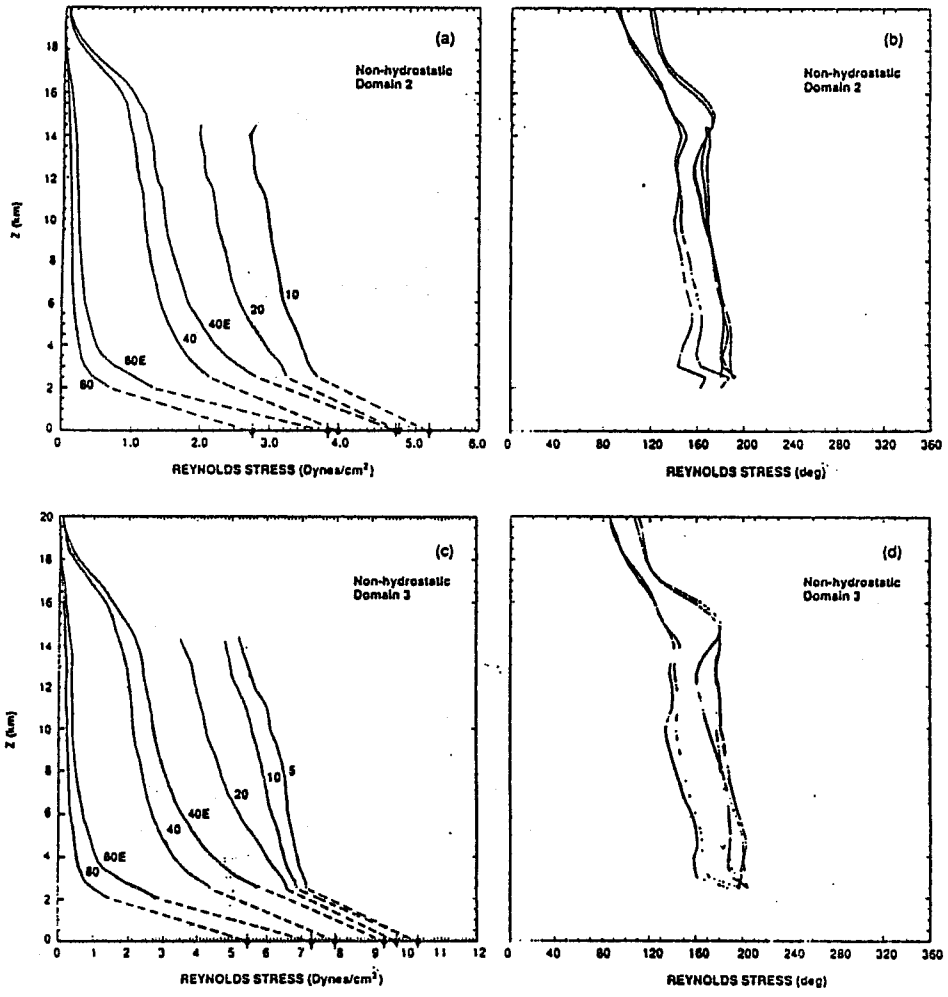

Fig. 9 Pressure drag and Reynolds stresses at $t = 600$ min corresponding to experiments shown in Fig. 6. As in Fig. 5 the dashed lines only indicate connection between stresses and drag values. Profiles marked with 'E' denote simulations using an envelope orography.

the pressure drag. The inclusion of a gravity wave drag parameterization in concert with the envelope orography should result in a similar level of improvement for the wave drag as occurred for the pressure drag.

7. SIMULATIONS OF THE FRONT RANGE OF THE ROCKY MOUNTAINS AIRFLOW

As part of a joint study between NCAR and NOAA scientists, Clark and Hall have carried out a number of simulations of the airflow over the Colorado Rockies. These simulations are performed in three dimensions covering most of the state of Colorado using Clarks non–hydrostatic model. Horizontal resolutions of 10 and 3.33 km are used for the coarse outer domain and inner domain, respectively. The vertical resolution was taken as 500 m for both domains. The inner domain was situated over the main divide of the Rockies from Wyoming in the North to New Mexico in the South. The east–west extent and height of the inner domain was chosen sufficient to encompass the region of breaking gravity waves forced by the underlying orography. The importance of wave breaking to the high drag state of forced orographic flow was shown by Peltier and Clark (1979, 1983) and generally accepted by most current modellers of this subject. These simulations were performed using varying degrees of surface friction. The initial or upstream conditions were taken to be in an Ekman balance in the lower levels and geostrophic balance above about 1 or 2 km.

The initial conditions for the model simulations were taken from the vertical profiles of wind, temperature and moisture from Craig Colorado on 9 Jan 1989. These conditions were strongly time dependent and this temporal behaviour was treated in the calculations. As an indication of the temporal behaviour of the windstorm Fig. 10 shows the wind versus time at Boulder from both the observations and one of the model simulations. The wave breaking region in the simulation was extensive and is shown in Fig. 11. It extends over the entire north–south extent of the inner domain. It is this region which is expected to be play a major role in the deposition and reflection of momentum associated with vertically propagating gravity waves.

Figure 12 shows a time series of the Reynolds stress for both the low drag case ($C_d = .001$) and the high drag case ($C_d = .01$).

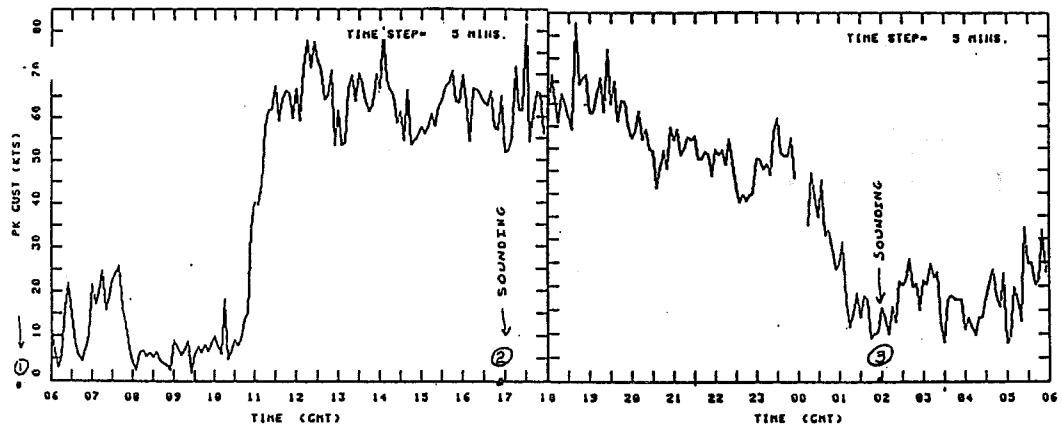

OBSERVATIONS

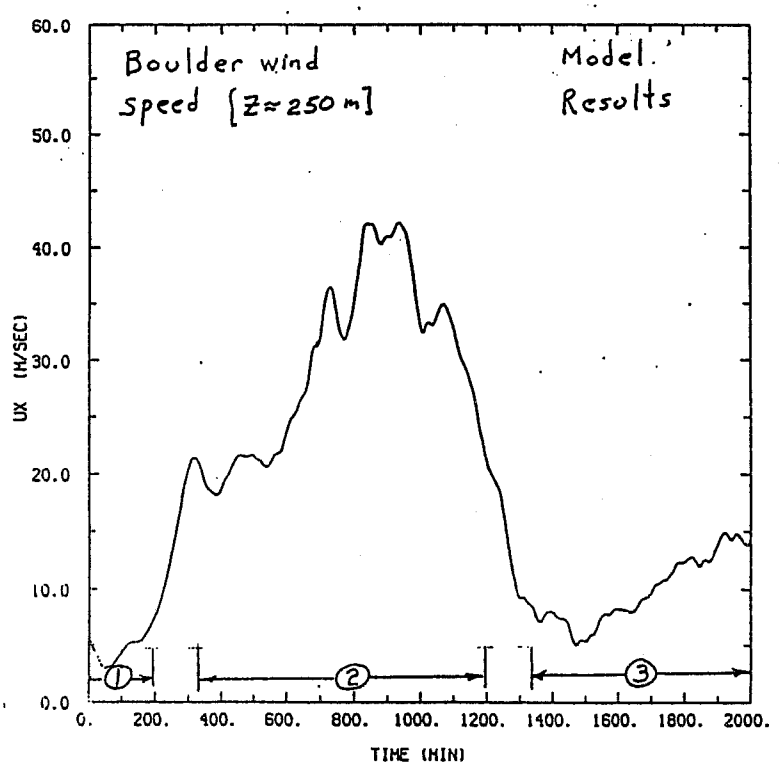

Fig. 10 Horizontal wind versus time. (a) observations from the NOAA building ($z \approx 30m$) in Boulder Colorado on 9 Jan 1989. (b) Model simulated wind versus time which represents a vertical average over a 500m grid increment.

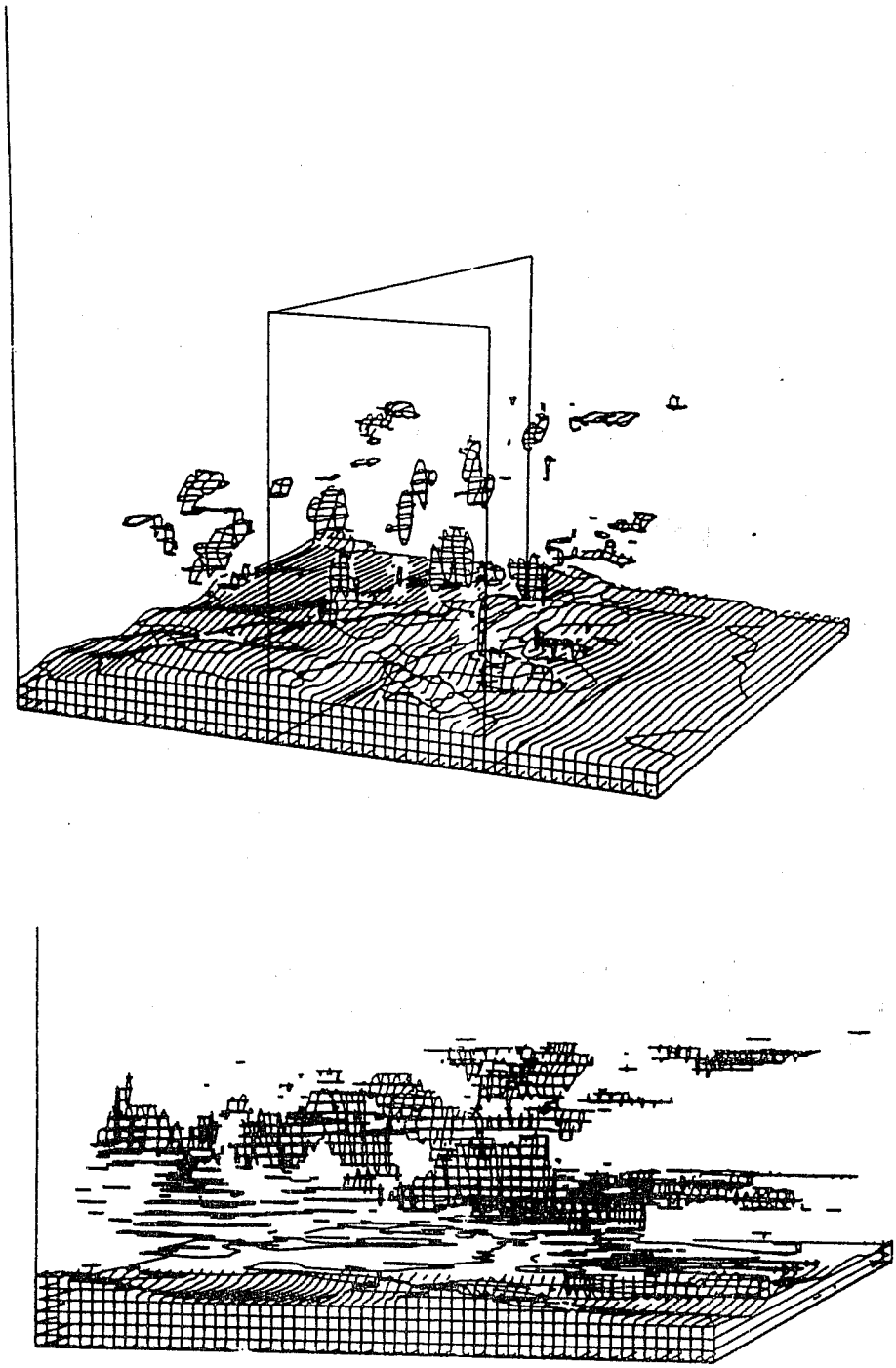

Fig. 11 Outline of the wave breaking region for the windstorm event of 9 Jan 1989 over the Colorado Rockies. Surface of $u < -10ms^{-1}$ are shown. Time is taken during an intensive drag period. (a) shows outer domain perspective and (b) the inner domain perspective.

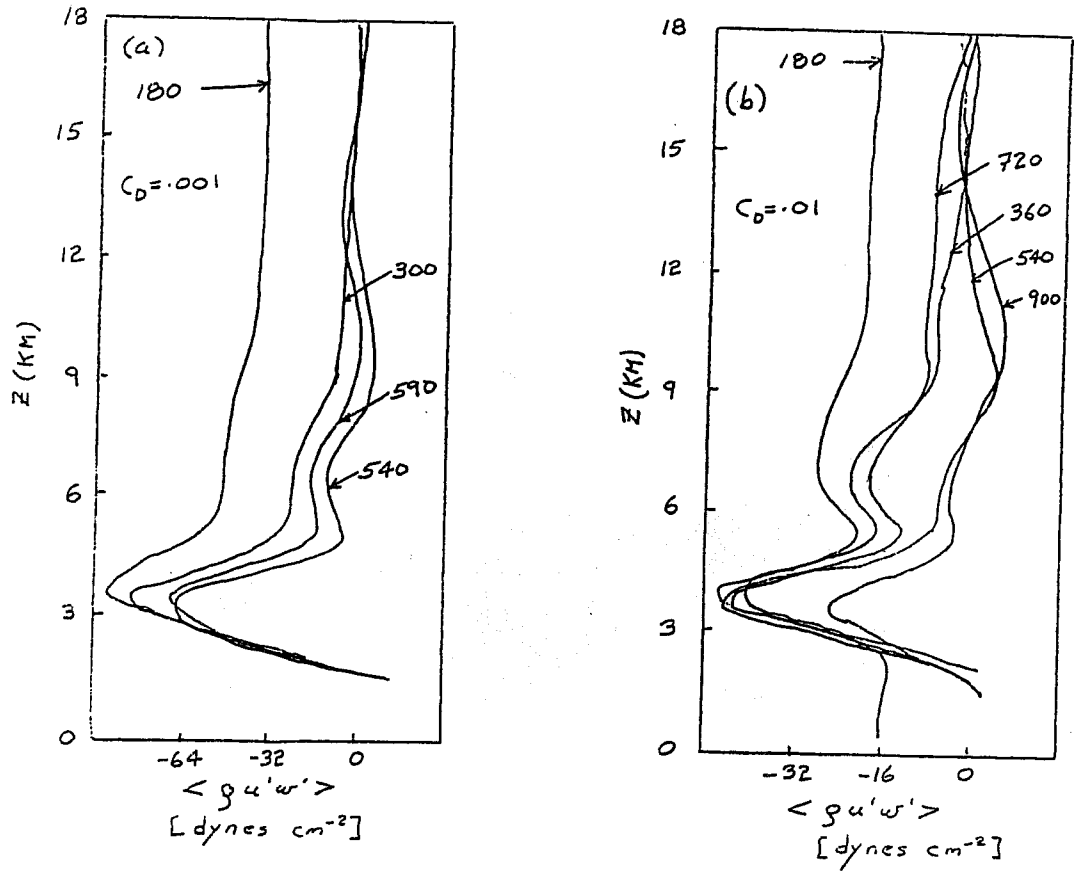

Fig. 12 Time series of Reynolds stress for the 9 Jan 1989 windstorm event over the Colorado Rockies. (a) for the low drag case using $C_d = .001$ and (b) for the high drag case using $C_d = .01$.

7. CONCLUSIONS

Comparisons between model simulations and observations of airflow over the Alps suggests a strong need for further studies of this type. The pressure drags appear to compare rather favourably with the observations and also appear to be rather insensitive to such physical effects as surface friction, although, there is a need for better estimates of the magnitude of the pressure drag due solely to surface friction. On the other hand, the momentum flux predictions do not as yet compare very well with the observations and they appear to be much more sensitive to such physical effects as surface friction.

The current trend in increasing memory size of the super computers allows for the possibility of using linear theory to further our understanding of finite amplitude orographic mountain flow. Matrix inversion techniques similar to those of Chen and Trenberth (1988) can be applied to steady–state gravity wave calculations of airflow over complex terrain satisfying the physically correct lower boundary conditions. The utility of such linear models might be assessed for studying the parameterization of drag as well as studying friction effects including no–slip conditions. The spectral content of the effective orography might be used to further our understanding of the dynamics of airflow over finite amplitude orography. The aliasing effect which shows up in the effective orography might be used to assess some sort of optimized filtering for the physical orography used in fully nonlinear models.

The simulations using envelope orography showed a significant improvement in model simulated pressure drag. It had little effect on wave drag as no wave drag parameterization was considered. Future resolution experiments such as these might consider both envelope and gravity wave drag parameterizations in concert as a type of verification test of such techniques.

REFERENCES

Boer, G.J. McFarlane, N.A., Laprise, R., Henderson, J.D., and J.-P. Blanchet, 1984: The Canadian climate centre spectral atmospheric general circulation model. *Atmos. Ocean*, **22**, 397–429

Bretherton, F.P., 1969: Momentum transport by gravity waves. *Quart. J. Roy. Meteor. Soc.*,**95**, 213–243.

Chen, S.-C. and K. E. Trenberth, 1988: Orographically forced planetary waves in the northern hemisphere winter: Steady state model with wave– coupled lower boundary formulation. *J. Atmos. Sci.*, **45**, 657–680.

Clark, Terry L., 1977: A small–scale dynamic model using a terrain–following coordinate transformation. *J. Comp. Phys.*, **24**, 186–215.

Clark, T. L., and W. R. Farley, 1984: Severe downslope windstorm calculations in two and three spatial dimensions using anelastic interactive grid nesting: A possible mechanism for gustiness. *J. Atmos. Sci.*, **41**, 329–350.

Clark, Terry L. and Martin J. Miller, 1991: Drag and Momentum Fluxes Forced by the Alps. Part II: Representation in Large-scale Atmospheric Models. *Quart. J. Roy. Meteor. Soc.*, (in press)

Hoinka, K.P. and Terry L. Clark, 1991: Pressure Drag and Momentum Fluxes Forced by the Alps. Part I: Comparison between Numerical Simulations and Observations. *Quart. J. Roy. Meteor. Soc.*, (in press)

Keller, T.L., M.G. Wurtele, and R.D. Sharman, 1991: Implications of the hydrostatic assumption on atmospheric gravity waves. To be presented at the 8th conference on atmospheric and oceanic waves and stability, Oct, Denver.

Laprise, R. and W.R. Peltier 1989: The linear Stability of Nonlinear Mountain Waves: Implications for the Understanding of Severe Downslope Windstorms. *J. Atmos. Sci.*, **46**, 545–564

Lilly, D.K., and J.B. Klemp 1979: The effects of terrain shape on nonlinear hydrostatic mountain waves. *J. Fluid Mech.*, **95**, 241–261

Mesinger, F. and Strickler, R.F. 1982: Effect of mountains on Genoa Cyclogenesis. *J. Meteor. Soc. Japan*, **60**, 326–338

Miles, J.W. and H.E. Huppert 1969: Lee waves in a stratified flow. Part 4. Perturbation approximations. *J. Fluid Mech.*, **35**, 497–525

Palmer, T.N., Shutts, G.J. and R. Swinbank, R., 1986: Alleviation of a systematic westerly bias in general circulation and numerical weather prediction models through an orographic gravity wave drag parameterization. *Quart. J. Roy. Meteor. Soc.*, **112**, 1001–1040

Peltier, W. R., and T. L. Clark, 1979: The evolution and stability of finite amplitude mountain waves – II: Mountain wave drag and severe downslope windstorms. *J. Atmos. Sci.*, **36**, 1499–1529

Peltier, W. R., and T. L. Clark, 1983: Non–linear mountain waves in two and three spatial dimensions. *Quart. J. Roy. M. S.*, **109**, pp. 527–548.

Richard, Evelyne, Patrick Mascart and Everett C. Nickerson, 1989: The Role of Surface Friction in Downslope Windstorms. *Journ. Applied Meteor.*, **28**, 241–251

Smith, R.B. 1976: The generation of lee waves by the Blue Ridge. *J . Atmos Sci.*, **33**, 507–519

Vergeiner, I., 1971: An operational linear lee wave model for arbitrary basic flow and two–dimensional topography. *Quart. J. R. Met. Soc.*, **97**, 30–60

Wallace, J.M., Tibaldi, S. and Simmons, A.J. 1983: Reduction of systematic forecast errors in the ECMWF model through the introduction of an envelope orography. *Quart. J. Roy. Meteor. Soc.*, **109**, 683–717